GENERAL ATOMIC

DIVISION OF

GENERAL DYNAMICS

JOHN JAY HOPKINS LABORATORY FOR PURE AND APPLIED SCIENCE

P.O. BOX 608, SAN DIEGO, CALIFORNIA 92112

GACD-5974

Copy No. 30

RADIATION EFFECTS ON SILICON

Second Quarterly Progress Report Covering the Period

September 1 through November 30, 1964

GPO PRICE $ _____

OTS PRICE(S) $ _____

Hard copy (HC) $1.00

Microfiche (MF) .50

Work done by:

L. A. Berry
S. K. Boehm
H. Horiye
H. K. Lintz
D. K. Nichols
D. P. Snowden
V. A. J. van Lint

Report written by:

H. K. Lintz
D. P. Snowden
V. A. J. van Lint

National Aeronautics and Space Administration
Contract No. NAS7-289
Project 430

December 14, 1964

I. INTRODUCTION

This second quarterly report on Contract NAS7-289, "Radiation Effects on Silicon," covers the period September 1 through November 30, 1964. During this period work was performed in the following areas.

1. Studies were made by ESR of the vacancy phosphorus center induced by 8 to 30 MeV electrons.

2. Measurements on n- and p-type silicon were made of carrier lifetimes by pulsed dc conductivity.

3. Measurements were made on n- and p-type silicon of the carrier lifetime by microwave reflection.

These topics will now be discussed in more detail.

II.   ESR MEASUREMENTS

2.1   INTRODUCTION

During this quarter measurements have continued on the centers produced by the irradiation of n-type phosphorus-doped floating-zone silicon. The primary data obtained from these measurements are values of the introduction rate of the vacancy-phosphorus defect produced by room-temperature irradiation at 8, 15 and 30 MeV. These results will be discussed below.

In addition one, and possibly two, previously unreported centers have been observed in 0.1 ohm-cm P-doped silicon irradiated at 300° K with 30 MeV electrons with fluxes between 3.7×10^{16} and 9.2×10^{16} cm^{-2}. The Fermi level in these samples is above that value for which the vacancy-phosphorus resonance is seen. Since no systematic study of these resonance signals has been made they will not be discussed further at this time.

2.2   EXPERIMENTAL TECHNIQUES

The experimental techniques used for the ESR measurements have been described previously.[1] In addition, it has become obvious that interpretation of the resonance results would be greatly simplified by a knowledge of the Fermi level position for each sample. (An example of this simplification is given above. The unidentified resonance signals reported in the introduction are known not to be due to either the vacancy-phosphorus center or the divacancy since Hall effect measurements have shown the Fermi level to be above the level at which these centers appear in spin resonance.) To this end, two approaches have been taken. Pairs of samples have been prepared and irradiated together, one for ESR measurements and a second with gold-bonded leads for Hall effect measurement. The temperature dependence of the Hall effect is measured with a standard dc technique in a magnetic field of ~ 4000 Oe. From the temperature dependence of the carrier concentration the Fermi level is obtained. For samples with the Fermi level well removed from the conduction band, the temperature dependence of the conductivity itself is sufficient to measure this level since the temperature dependence of the mobility is small compared with that of the carrier concentration. This measurement is made on the ESR samples themselves using a four-point probe method with phosphor bronze contacts to the sample.

These Fermi level measurements have only recently begun but will be used regularly to complement the resonance measurements.

2.3 RESULTS AND CONCLUSIONS

2.3.1 The Vacancy-Phosphorus Center

The vacancy-phosphorus complex, the E-center, or adopting a new terminology introduced by Watkins, [2] the G-8 center, is seen by spin resonance when the Fermi level is below the energy of the center, i.e., below E_C - 0.4 eV. For this reason the number of G-8 centers* is not a linearly increasing function of flux, but instead only begins to increase as the Fermi level approaches the energy of the center. There are thus two, and possibly three, introduction rates associated with the vacancy-phosphorus complex: 1) the introduction rate of the negatively charged complex (which is not directly observed), 2) the rate of appearance of G-8 centers as the Fermi level moves through the E_C - 0.4 eV level, and 3) (provided E_F < E_C - 0.4 eV before all phosphorus atoms have a vacancy associated with them) the rate of introduction of the uncharged vacancy-phosphorus, which may be different than that for the charged state.

Our data are not yet sufficiently precise to distinguish differences between these rates. The introduction rates shown in Table 1 are calculated from the maximum G-8 center concentration obtained and the flux necessary to obtain that concentration. Also shown in the table are the number of samples irradiated and the range of flux covered. The values for the introduction rate quoted in the table should be accurate to within a factor of 2.

Two experimental difficulties associated with measurement of the vacancy-phosphorus introduction rate should be mentioned. Because the G-8 center appears at flux levels at which other centers are produced,

---

*By G-8 center we specifically mean the underlined_uncharged vacancy-phosphorus defect, i.e., that center observed in spin resonance. The singly-negatively charged center, which prevails with E_F > E_C - 0.4 eV is not implied except when specifically named.

Table 1

Energy (MeV)	Number of Samples Irradiated	Range of Fluxes (cm^{-2})	Introduction Rate (cm^{-1})
8	5	2.7 to 5.3 x 10^{17}	0.03
15	4	3.1 to 6.1 x 10^{17}	0.03
30	4	2.0 to 5.3 x 10^{17}	0.06
Approximate vacancy-phosphorus introduction rates			

careful identification of the resonance peaks associated with the G-8 center is necessary in order that a correct determination of the intensity can be made. Second, area measurements are complicated when lines of different centers overlap. By measurements of the orientation dependence of the observed resonances, it is possible to identify the signals due to the G-8 center and also to choose orientations at which overlap is a minimum. The area determinations are also aided by a knowledge of the theoretically expected relative intensities of the G-8 center lines. Completion of such orientation dependence studies on the samples used to obtain the energy dependence of the introduction rate should considerably improve the accuracy of those results.

Finally it should be mentioned that a slight discrepancy exists between the g-values obtained in the present study and those reported by Watkins and Corbett[3] for the G-8 center. Our results can best be fitted by values for the g-tensor 0.0005 below those given in the above reference. However, Watkins and Corbett quote an accuracy of $\pm$ 0.0003 and we estimate a similar accuracy, so that our measured values do overlap. It is almost certain that the difference between the results is due to a systematic error, and that we are indeed measuring the same center. The evidence for this conclusion is strong. We see identical orientation dependence to that reported by Watkins and Corbett and our Hall effect results indicate that the resonance appears with $E_F \approx E_C - 0.4$ eV.

2.4 FUTURE WORK

Measurements of the vanancy-phosphorus introduction rates will be completed by careful orientation-dependent intensity measurements. Depending on the exact nature of these results, measurements at other irradiation energies may be performed. If the results are sufficiently accurate, theoretical studies of the shape of the G-8 center concentration curve as a function of flux may be performed. Such studies could yield the production rate of deeper centers responsible for pulling the Fermi level below the G-8 center level.

Studies will begin on the production rate of the divacancy in p-type material to extend the recent work of Watkins and Corbett.[4]

III. CARRIER LIFETIME MEASUREMENTS

Recent carrier lifetime measurements have been performed by two techniques: (1) pulsed dc conductivity and (2) microwave reflection. Method (1) has been described previously.[5] Method (2) has the advantage that electrical contacts are not required on the sample. Hence, the problems with rectifying contacts, especially at low temperatures, are avoided. Unfortunately, the microwave method appears to be amenable to measurements over a more limited dynamic range in excess conductivity than the pulsed dc method. Hence, it will be used to check the pulsed dc method for errors that may be introduced by the contacts, but it cannot supplant the earlier method.

The following specific lifetime measurement experiments have now been performed.

1. Irradiated 7 ohm-cm, floating-zone, P-doped n-type silicon was studied over a large range of excess-carrier concentration with the pulsed dc method from 100° to 400°K. The data films have been read and partially processed by the computer.

2. Irradiated 7 ohm-cm, floating-zone, B-doped p-type silicon was studied at the higher injection levels from 100° to 400°K. The films are being read in preparation for computer processing. This experiment was very difficult due to contact rectification problems and was unsuccessful on the first two attempts. It will be repeated in the near future with larger resistance in series with the sample to further decrease the effects of contact resistance.

3. Irradiated 7 ohm-cm floating-zone P-doped n-type silicon and 7 ohm-cm floating-zone B-doped p-type silicon were studied from 100° to 300°K with the microwave method. The results have been analyzed but are uncertain due to the subsequent discovery of inadequate thermal contact between the sample and the temperature-controlled waveguide. Hence, this measurement will be repeated with the same irradiated samples with better temperature control.

One significant improvement in technique has been effected in the computer data reduction. The program has been modified so that the computer performs a least squares adjustment of an exponential curve to short

sections of each decay curve. As a result, each measurement results in
~ 5 decay constants for the same number of constants for the same number
of different excess-carrier densities. Hence it is no longer necessary to
perform extensive plotting of the decay curves and curve fitting, since
the τ values can be plotted directly as τ ($1 + \Delta n/n_0$) versus $\Delta n/n_0$. An
example of such data is shown in Fig. 1. The behavior expected from the
Shockley-Read formula is shown, and the deviation noted previously[5] at
low excess-carrier concentrations is now clearly apparent.

The experiments have also been improved markedly. Measurements are
now taken rapidly at a large number of temperatures to form a continuous
curve of $\tau(T)$. Some improvements in the measuring circuit have also
decreased the rf noise interference, allowing measurements of short decay
times to be performed more accurately.

3.1 MEASUREMENTS BY MICROWAVE REFLECTION ON SILICON

In order to avoid the contact problems which are encountered by
measuring excess-carrier lifetimes in semiconductors, a microwave method
was applied in which the reflected microwave power from an electrodeless
sample was used to measure the transient conductivity. In this method,
the complex propagation constant is measured as a function of time using
a reflected microwave signal as the probe. Cavity methods could not be
applied since they involve approximations not valid in cases of high loss
samples, and the method of measuring transmissions through a sample in a
waveguide seemed inconvenient since the sample has to be maintained at
cryogenic temperatures.

The microwave circuit used for these measurements is demonstrated
in Fig. 2. The microwave energy comes from a klystron and goes through
isolator 1 and through an adjustable attenuator. After the attenuator
a small fraction of the power is coupled into a cavity, the resonance
absorption of which is detected at crystal 1 and used for frequency
stabilization of the klystron. The main microwave power goes through
isolator 2 into the magic T and into the reflection bridge respectively.
A tunable microwave filter is introduced between the crystal on the magic T
and the magic T. This tunable microwave filter was introduced in order
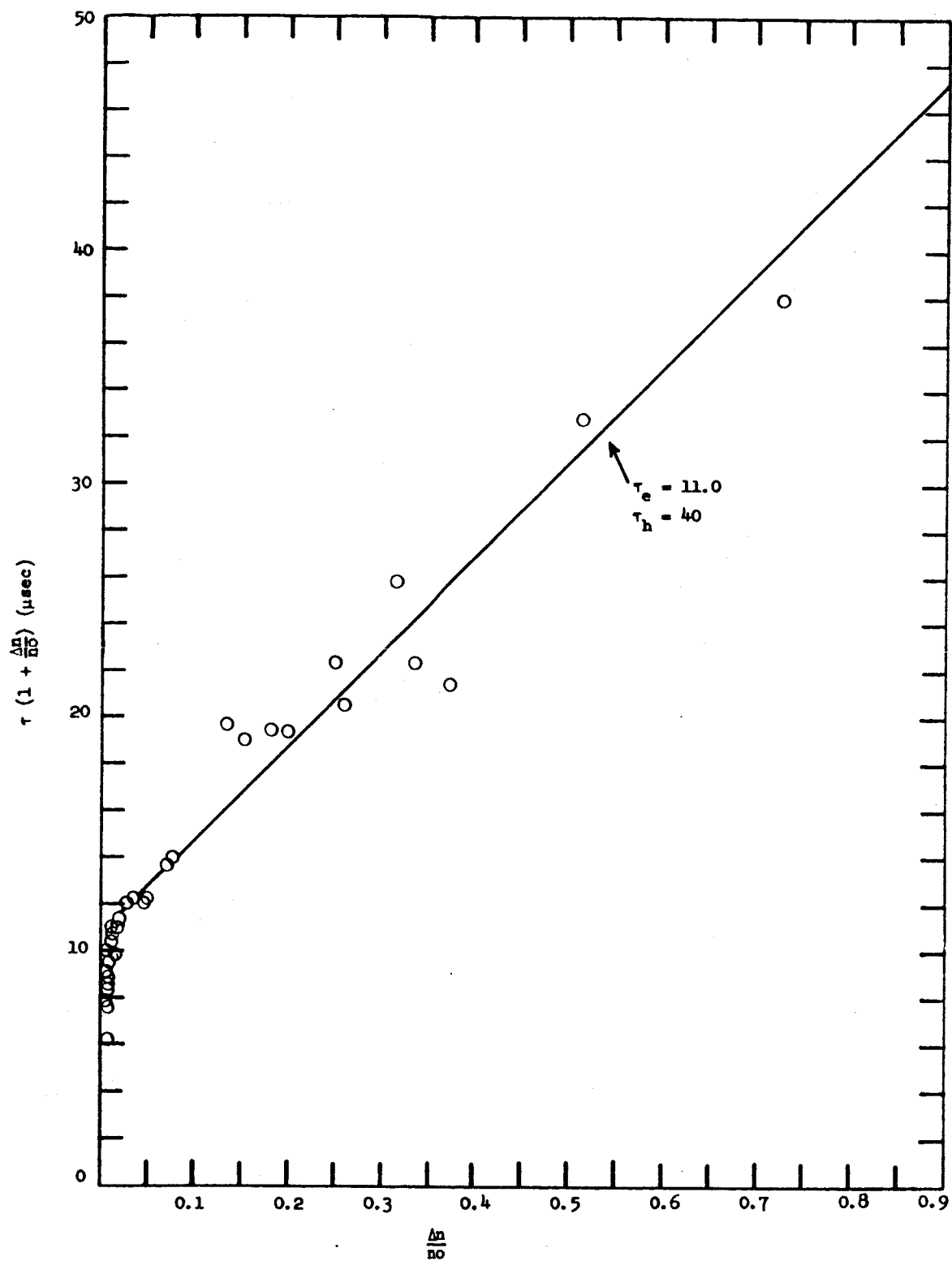to suppress microwave signals generated by the electron beam penetrating

7

$\tau\left(1 + \frac{\Delta n}{n_0}\right)$ (μsec)

$\tau_e = 11.0$
$\tau_h = 40$

$\frac{\Delta n}{n_0}$

Fig. 1--Dependence of τ on Δn in 7 ohm-cm floating-zone
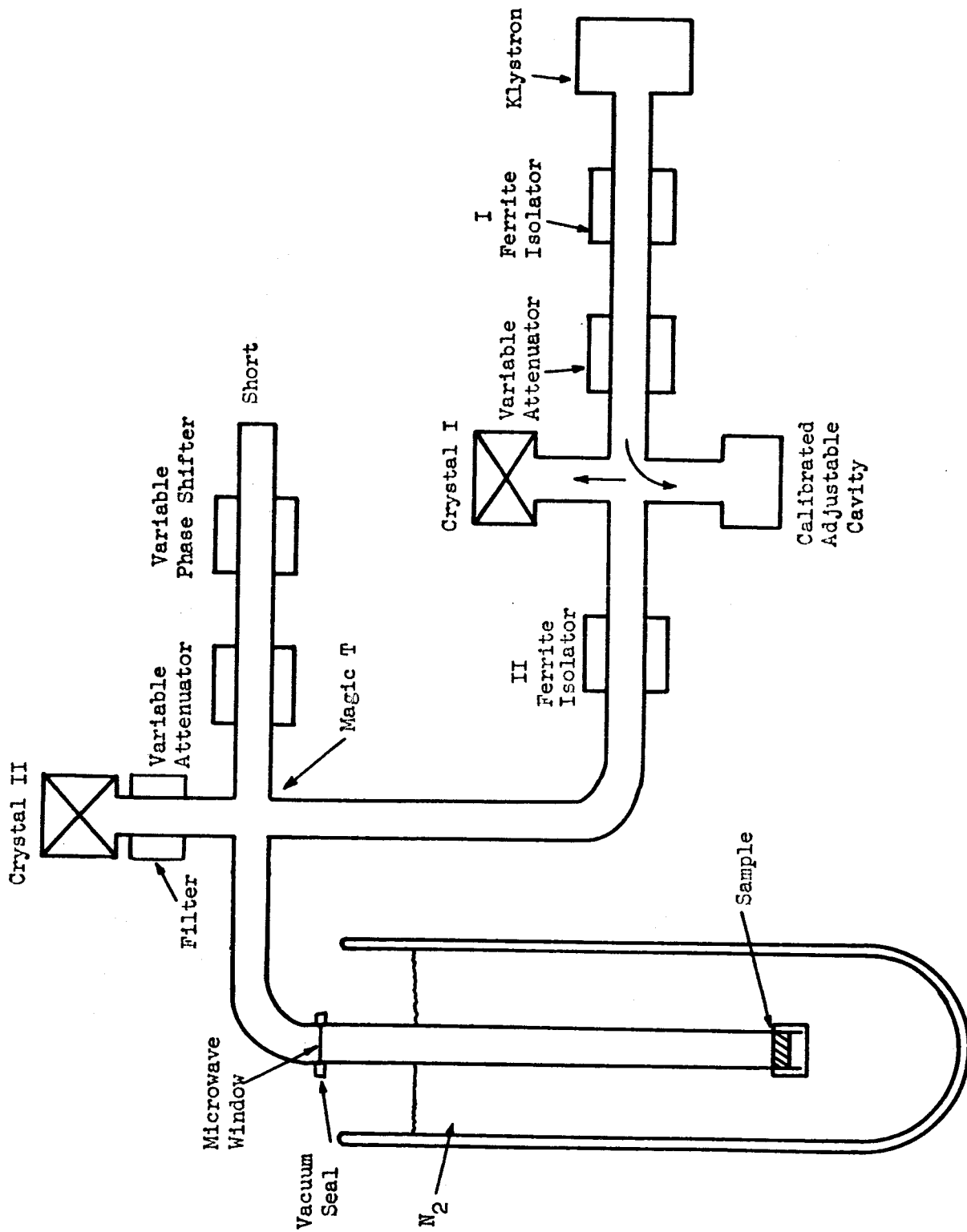P-doped unirradiated n-type silicon at 296°K

Fig. 2--Microwave circuit

the waveguide at the sample location. The microwave frequency was chosen to be between harmonics of the frequency generated by the Linac electron beam. The sample was located at the shorted end of the sample arm covering the total cross section of the waveguide. The last 20 inches of the sample arm formed a gas-tight chamber which could be evacuated in order to avoid condensation of air at liquid nitrogen or liquid helium temperatures. The temperatures were measured by means of a carbon resistor and a copper-constantan thermocouple, both of which were attached to the outside of the waveguide. The resistor and the thermocouple were both somewhat shielded against intimate contact with the bath in order to give more realistic values of the sample temperature. The sample arm of the reflection bridge reached down into the liquid helium glass dewar which could be emptied by remote control. The bridge signal was detected at crystal 2. Measurements could be made to determine both the phase shift and amplitude change in the signal reflected from the sample arm of the microwave circuit, but for the mere measurement of lifetimes the phase information was not required.

3.1.1 Theory

Consider propagation of a microwave in a waveguide with a semiconductor sample inserted at the end as shown in Fig. 3.

We are concerned with a rectangular waveguide ($\Delta X = a$; $\Delta Y = b$; $a > b$) operating in the TE_{10} mode only. The field for this mode is

$$E_Y = E_o \sin \frac{\pi X}{a} \, e^{i\omega t - \tilde{\Gamma} Z}$$

$$B_X = \frac{i}{\omega} \tilde{\Gamma} E_o \sin \frac{\pi X}{a} \, e^{i\omega t - \tilde{\Gamma} Z}$$

$$B_Z = \frac{i}{\omega} \frac{\pi}{a} E_o \cos \frac{\pi X}{a} \, e^{i\omega t - \tilde{\Gamma} Z}$$

$$\tilde{\Gamma}^2 = \left(\frac{\pi}{a}\right)^2 - \omega^2 \mu\epsilon + i\omega\mu\tilde{\sigma}.$$

Considering the geometry of (Fig. 3) with a vacuum in region I with $\epsilon = E_o$; μ_o, and $\tilde{\sigma} = 0$ and a semiconductor in region II with $\epsilon = \gamma \epsilon_o$, $\mu = \mu_o$; $\tilde{\sigma} \neq 0$ and the microwave propagating in the positive Z-direction, we find for the field in the two regions:
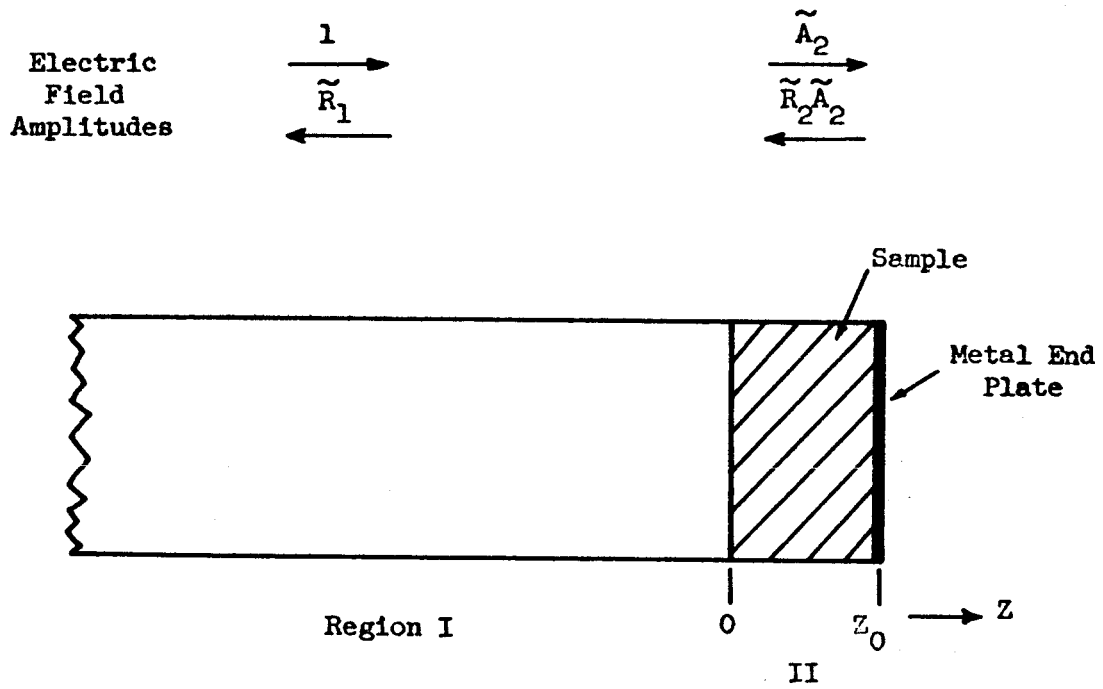
10

Electric
Field
Amplitudes

$$\xrightarrow{1}$$

$$\xleftarrow{\tilde{R}_1}$$

$$\xrightarrow{\tilde{A}_2}$$

$$\xleftarrow{\tilde{R}_2\tilde{A}_2}$$

Sample

Metal End
Plate

Region I

0

Z_0

$\longrightarrow$ Z

II

Fig. 3 --Waveguide and sample geometry

Region I:
$$E_Y = E_0 \sin\frac{\pi X}{a}\, e^{i\omega t}\left(e^{-\tilde{\Gamma}_1 Z} + \tilde{R}_1 e^{+\tilde{\Gamma}_1 Z}\right) \qquad Z \leq 0$$

$$B_X = E_0 \frac{i}{\omega}\tilde{\Gamma}_1 \sin\frac{\pi X}{a}\, e^{i\omega t}\left(e^{-\tilde{\Gamma}_1 Z} - \tilde{R}_1 e^{+\tilde{\Gamma}_1 Z}\right)$$

Region

$$E_Y = E_0 \sin\frac{\pi X}{a}\, e^{i\omega t}\left(\tilde{A}\, e^{-\tilde{\Gamma}_2 Z} + \tilde{R}_2 \tilde{A}_2\, e^{+\tilde{\Gamma}_2 Z}\right)$$

$$Z \geq Z \geq 0$$

$$B_X = E_0 \frac{i}{\omega}\tilde{\Gamma}_2 \sin\frac{\pi X}{a}\, e^{i\omega t}\left(\tilde{A}_2\, e^{-\tilde{\Gamma}_2 Z} - \tilde{R}_2 \tilde{A}_2\, e^{+\tilde{\Gamma}_2 Z}\right)$$

$\tilde{R}$ is the complex reflection coefficient.

With the boundary conditions:

$$E_Y (Z = Z_0) = 0$$

$$E_Y (0)\ (\text{region I}) = E_Y (0)\ (\text{region II})$$

$$B_X (0)\ (\text{region I}) = B_X (0)\ (\text{region II}),$$

we find for $\tilde{R}_1$

$$\tilde{R}_1 = \frac{\tilde{\Gamma}_1 - \tilde{\Gamma}_2 \coth \tilde{\Gamma}_2 Z_0}{\tilde{\Gamma}_1 + \tilde{\Gamma}_2 \coth \tilde{\Gamma}_2 Z_0} = \tilde{R}_1(\tilde{\sigma}).$$

We are not interested in $\tilde{A}_2$ or $\tilde{R}_2$ since $\tilde{R}_1$ is all we measure.

3.1.2 Experimental Results

An experiment was performed with a sample of n-type silicon having a room temperature resistivity of 10 ohm-cm cut to a thickness of 1 mm, to fit the end of the waveguide section. Measurements were made over the temperature range between room temperature and liquid nitrogen temperature. The data have been analyzed and the measured lifetimes for high and low intensity Linac pulses are plotted versus 1/T in Figs. 4a and b.

A consistency check on the transient conductivity revealed a deviation of the measured |R| from the theoretically possible calculated |R|.

A very careful study of the microwave bridge showed that, because of multiple reflections from various components and a small power leakage at the magic T from the power input arm into the crystal arm, the signal received at the crystal was distorted.
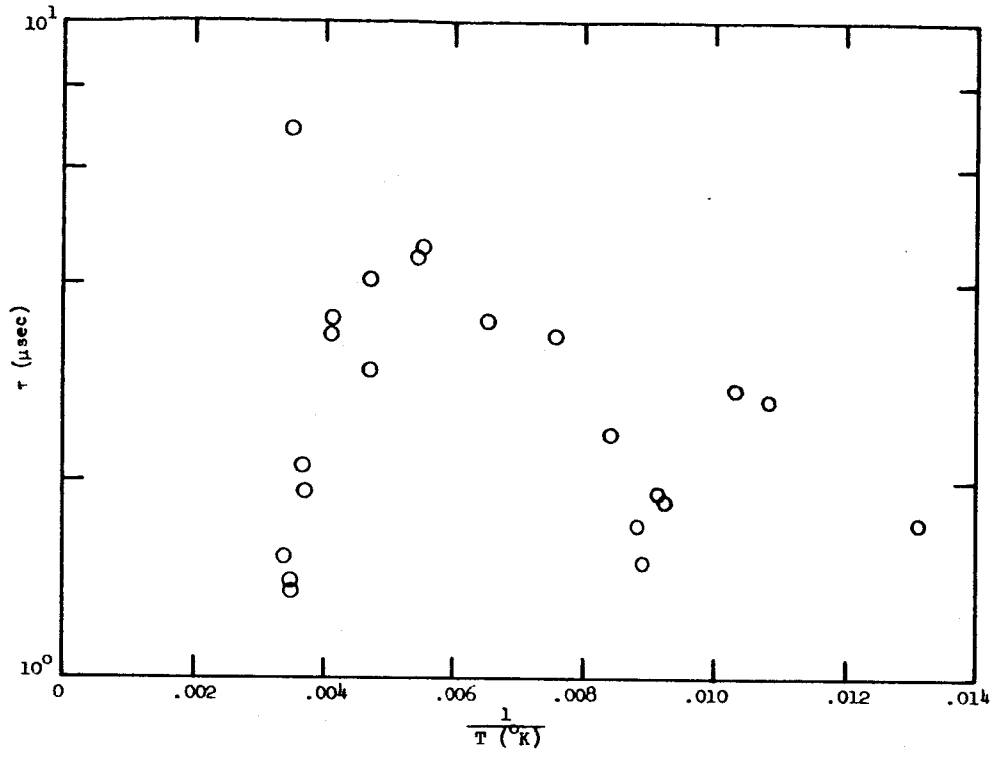
12

Fig. 4a--Lifetimes versus inverse temperature at high-intensity electron pulses
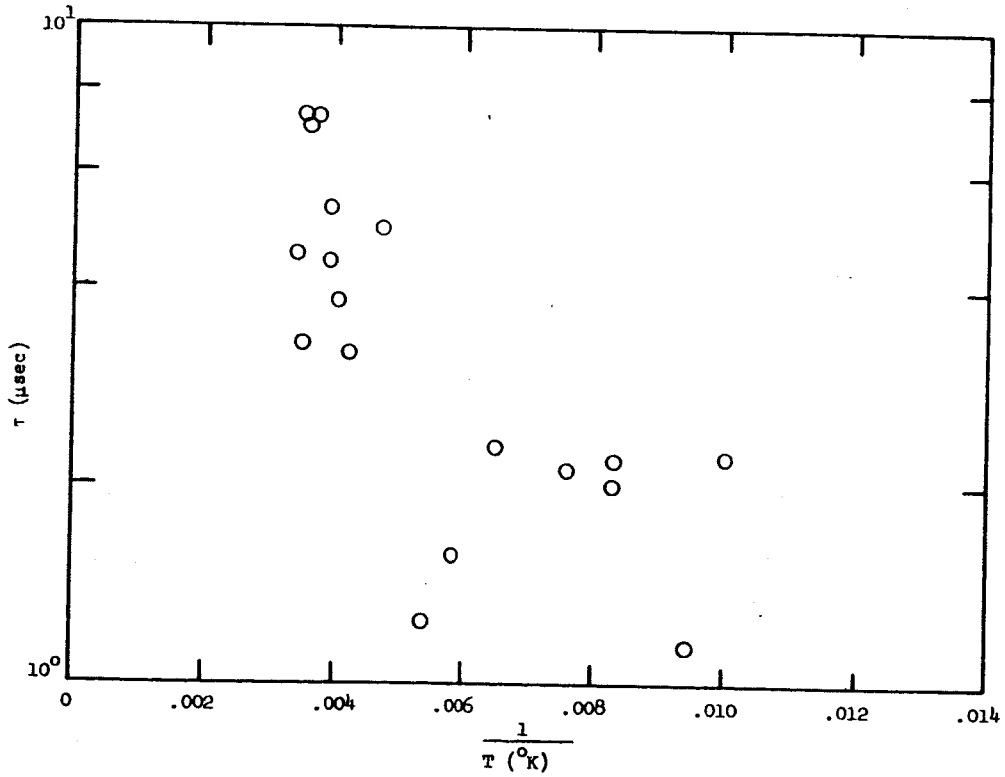

Fig. 4b--Lifetimes versus inverse temperature at low-intensity electron pulses

13

Based on these findings it was decided to use a slightly modified measuring circuit, and to use a different crystal calibration procedure. Also the sample arm was re-designed so that the contact between the waveguide walls and the semiconductor as well as the temperature measurement would be improved.

The new circuit is shown in Fig. 5. In this modified circuit, the microwave generator feeds power into the magic T. Entering the magic T the power is split in two halves, one half going into the reflectionless, absorber and the other half going into the sample arm. The connection between the sample arm and the magic T consists of a phase shifter and a directional coupler which deflects 10% of the incident power into the waveguide arm containing crystal number 2. Thus the incident power can be monitored by crystal number 2. The arm on which crystal number 2 is mounted consists of the isolator and a microwave filter. The main part of the microwave power will then go into the actual sample arm and then be partially reflected from the sample back to the magic T. At the magic T, the reflected signal again is split into two halves, only one of which reaches crystal number 1. Since we now measure the incident power on the sample and the reflected power simultaneously, the absolute value of the reflection coefficient can be determined independent of possible fluctuations of the generator power output. One requirement is, however, that the two crystals be calibrated simultaneously while in the circuit so that the effect of the remaining small reflections originating from bends, windows, isolators, filters and crystal holders are all included in the calibrations, and that the phase shifter is tuned for maximum quiescent signal, so that a signal phase shift interacting with the leakage power causes a minimum signal change. The theory concerning the reflection coefficient as a function of the conductivity, σ, is the same as the one described above.

The sample holder is shown in Fig. 6. The holder consists of a waveguide which is inserted into a vacuum-tight stainless steel sheath. The sample is soldered into the waveguide and metal plated on the outside to form a perfect short on the end of the waveguide. The thermocouple is attached to the sample underneath the metal plating. A styrofoam plug prevents the sample from facing metal parts of the upper waveguide and
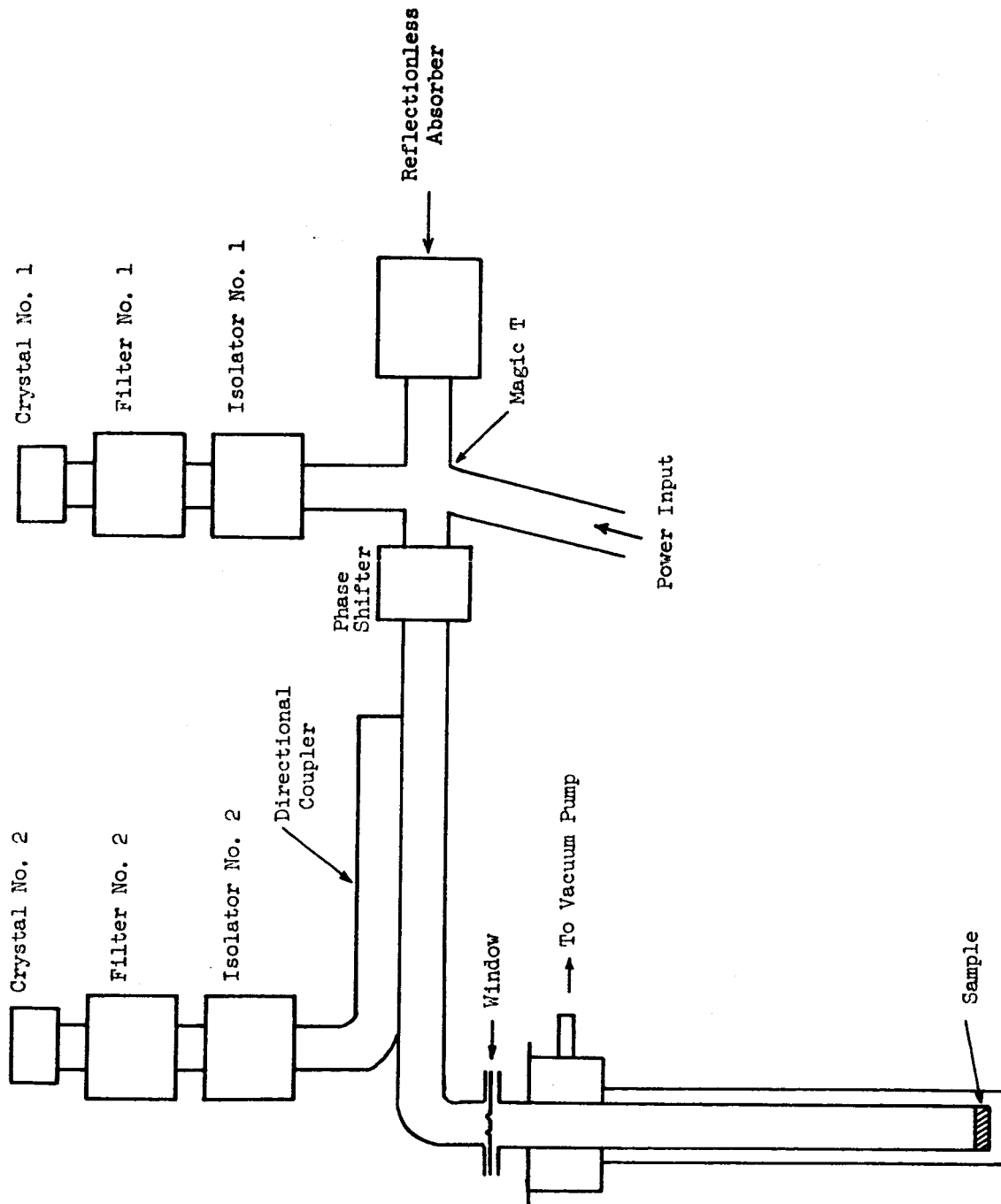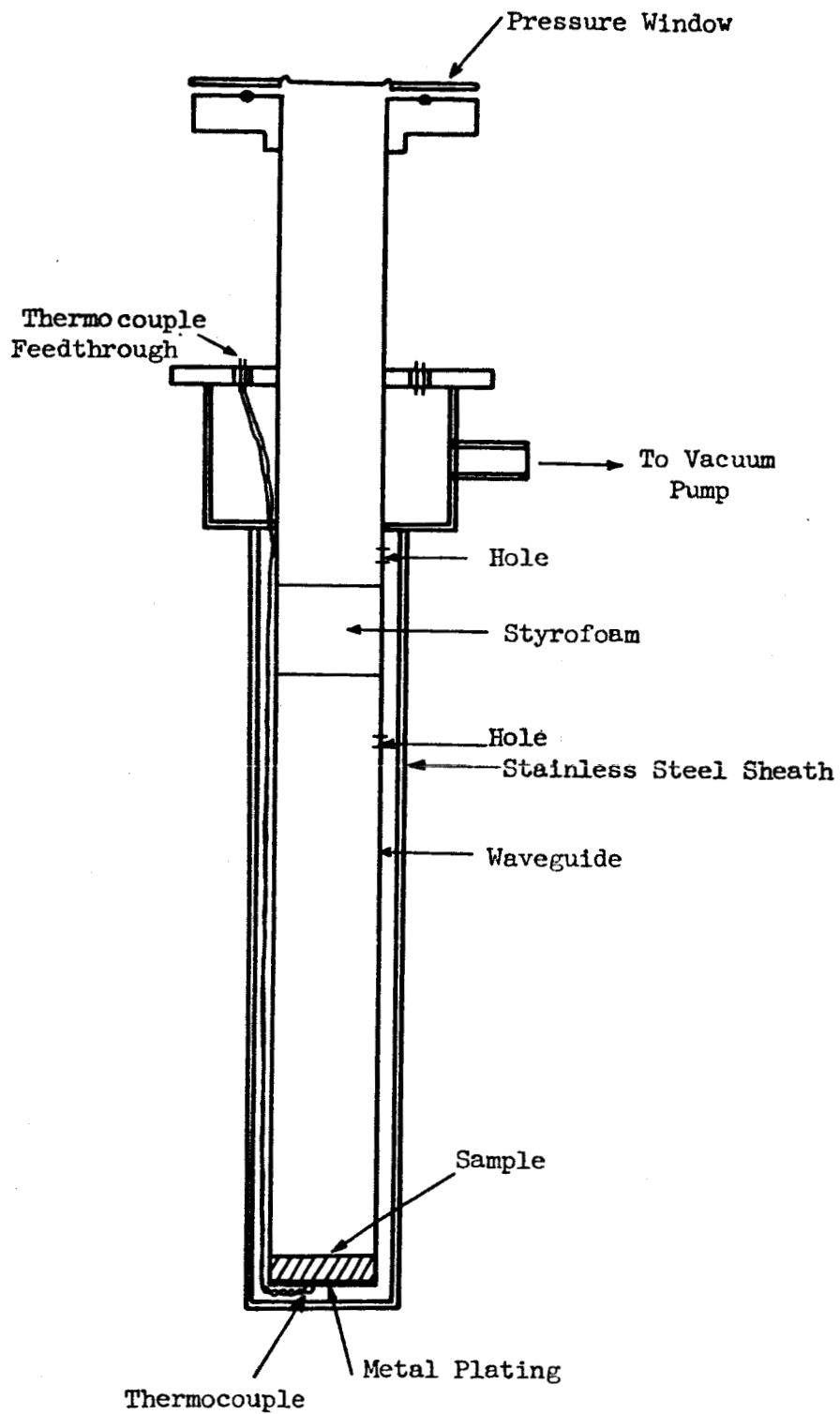
Fig. 5--Modified circuit

Fig. 6--Sample holder configuration

thus from warming up too much through heat radiation from these parts. Two 1/16" holes drilled in the center of the waveguide in the direction of the electrical vectors, one above and one below the styrofoam plug, assure that the waveguide can be evacuated together with the sheath by pumping on the outlet. This is to avoid the condensation of oxygen and nitrogen inside the waveguide at very low temperatures.

Experiments with the improved measuring arrangements are beginning now.